Electron Paramagnetic Resonance Analysis of a Transient Species Formed During Water Oxidation Catalyzed by the Complex Ion [(bpy)$_2$Ru(OH$_2$)]$_2$O^{4+}

Jamie A. Stull,[§] Troy A. Stich,[§] James K. Hurst,[‡] and R. David Britt*,[§]

[§]Department of Chemistry, University of California–Davis, One Shields Avenue, Davis, California 95616, United States
[‡]Department of Chemistry, Washington State University, Pullman, Washington 99164-4630, United States

Ⓢ Supporting Information

ABSTRACT: The ruthenium "blue dimer" [(bpy)$_2$Ru-(OH$_2$)]$_2$O^{4+}—the first well-defined molecular complex able to catalyze water oxidation at low overpotentials—has been the subject of numerous experimental and computational studies. However, elements of the reaction mechanism remain controversial. Of particular interest is the nature of the O–O bond-forming step. Herein, we report the first advanced electron paramagnetic resonance (EPR) spectroscopic studies of a high-valent intermediate that appears under conditions in which the catalyst is actively turning over. Results from previous studies have suggested that this intermediate is derived from [(bpy)$_2$Ru^V(O)]$_2$O^{4+}, denoted {5,5}. Under photooxidizing conditions, the corresponding EPR signal disappears at a rate comparable to the turnover rate of the catalyst once the illumination source is removed. In the present work, the electronic and geometric structures of this species were explored using a variety of EPR techniques. Continuous wave (CW) EPR spectroscopy was used to probe the hyperfine coupling of the Ru ions, while corresponding ligand ^{14}N hyperfine couplings were characterized with electron spin echo envelope modulation (ESEEM) and hyperfine sublevel correlation spectroscopy (HYSCORE) methods. Finally, ^{1}H/^{2}H ENDOR was performed to monitor any exchangeable protons. Our studies strongly suggest that the accumulating transient is an $S = 1/2$ species. This spin state formulation of the so-called {5,5} species is consistent with only a limited number of electronic structures, each of which is discussed. Notably, the observed large metal hyperfine coupling indicates that the orbital carrying the unpaired spin has significant ruthenyl-oxyl character, contrary to an earlier electronic structure description that had tentatively assigned the signal to formation of a bipyridine ligand radical.
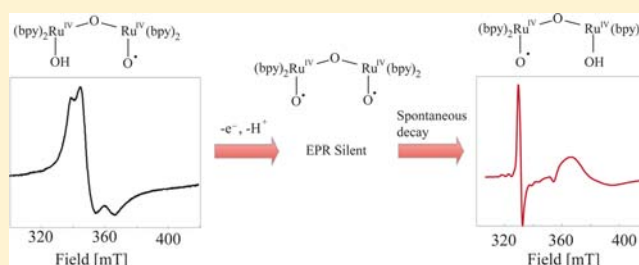
INTRODUCTION

Technologies that mimic the light-driven water-oxidation reaction catalyzed by photosystem II (PSII) are some of the leading candidates for addressing our growing energy needs.[1–4] Particular emphasis has been placed on producing functional models of the PSII active site, an inorganic cluster composed of four Mn ions and one Ca ion. This oxygen evolving complex stores four oxidizing equivalents (corresponding states termed S$_0$–S$_4$) prior to stripping two water molecules of four electrons and forming an O–O bond.[5–7]

The μ-oxo-bridged ruthenium "blue dimer" [(bpy)$_2$Ru-(OH$_2$)]$_2$O^{4+} (bpy = 2,2′-bipyridine) was the first well-defined molecular complex to be able to catalyze water oxidation at relatively low overpotentials.[8–10] Since then a large number of synthetic water-oxidizing complexes have been developed.[11–15] Despite these advances, an accurate description of the reaction mechanism of the blue dimer remains an unsatisfied goal.[16–19]

Analogous to the four-electron oxidation cycle of PSII, the ruthenium blue dimer is believed to store four oxidizing equivalents prior to oxygen evolution. The [(bpy)$_2$Ru^{III}(OH$_2$)]$_2$O^{4+} ion (hereafter denoted {3,3} to

indicate the formal oxidation state on the metal centers) is the lowest stable oxidation state of the dimer, equivalent to S$_0$, the most reduced state in the catalytic cycle of PSII.[20] The highest achievable oxidation state of the blue dimer was found to be {5,5}, attained by oxidation using rapid constant potential electrolysis (CPE) and assayed colorimetrically using [Os-(bpy)$_3$]$^{2+}$.[21] Based upon comparisons of rates of O$_2$ evolution and {5,5} decay to lower oxidation states, it was also evident that oxidation to this level was required for catalytic water oxidation.[21] Results from potentiometric and resonance Raman (RR) studies showed that four sequential one-electron oxidations coincide with deprotonation of coordinated water molecules until the {5,5} state is achieved, at which point complete deprotonation has occurred to give terminal oxo moieties.[20,21] Consequently, the molecular formula for {5,5} is [(bpy)$_2$Ru^V(O)]$_2$O^{4+}.[21] Driving the oxidizing potential more positive than that required to generate {5,5} leads to aqueous solvent breakdown at neutral pH.[20,22,23] In addition, spectro-

scopic results indicate that the stable {3,3} and {3,4} oxidation states contain dissociable protons on their aquo ligands.[20,21] Above pH 2, the reaction proceeds as follows: $\{3,3\} \xrightarrow{1e-} \{3,4\}$ $\xrightarrow{2e-} \{4,5\} \xrightarrow{1e-} \{5,5\}$. Below pH 2, {4,5} is unstable with respect to disproportionation, and the {4,4} form accumulates as a detectable intermediate, leading to an alternative reaction series: $\{3,3\} \xrightarrow{1e-} \{3,4\} \xrightarrow{1e-} \{4,4\} \xrightarrow{2e-} \{5,5\}$.[22]

Single crystal X-ray crystallographic data and electrochemical measurements of the {3,3} form in strongly acidic solutions are consistent with a $(H_2O)Ru^{III}-O-Ru^{III}(OH_2)$ core.[20,24,25] Low-temperature spectroscopic data indicate that {3,3} has an $S = 0$ ground state with a low-lying $S = 1$ excited state.[9,24,26,27] Distorted octahedral d^5 Ru^{III} ions are characteristically low-spin, which leads to each ion having a site spin of $S_{Ru(III)} = 1/2$.[28−31] These results point to the formulation of {3,3} as arising from two weakly antiferromagnetically coupled Ru^{III} ions. This oxidation state does not give rise to a cryogenic electron paramagnetic resonance (EPR) signal. In contrast, the one-electron oxidized {3,4} ion has a broad rhombic EPR signal centered at $g \approx 1.78$, suggestive of an $S = 1/2$ ground state (Figure 1A).[21,22,32] This EPR signal could arise from a strongly
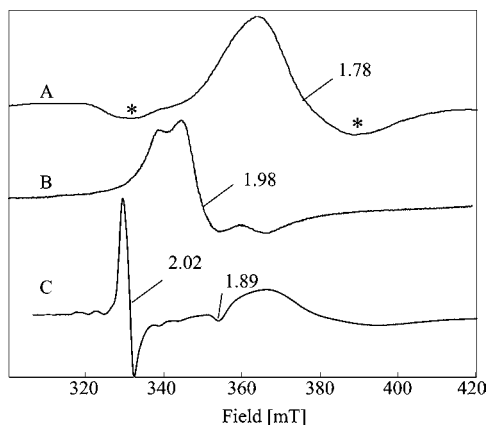
Figure 1. CW EPR spectra of the blue dimer collected at X-band microwave resonance frequencies (9.37 GHz). Spectrometer setting: temperature = 10 K; modulation amplitude = 8 mT; modulation frequency = 100 kHz; microwave power = 6.32 mW. (A) {3,4} at pH 9 in boric acid prepared by oxidation of {3,3} with sodium persulfate. This method of preparation led to background signals that could not be subtracted (indicated by asterisks on either side of the $g = 1.78$ signal). (B) {4,5} prepared by constant potential electrolysis (CPE) in 100 mM phosphate, pH 7.2;[22] (9.69 GHz) C) {5,5} solutions prepared by Ce^{4+} in 0.1 M CF_3SO_3H.[21]

coupled interaction between a Ru^{III} ($S_{Ru(III)} = 1/2$) center and a Ru^{IV} ($S_{Ru(IV)} = 1$) center. Alternatively, Ru^{IV} could be low-spin ($S_{Ru(IV)} = 0$) and the observed EPR signal would result from an isolated Ru^{III} center.[33,34] An $S_{Ru(IV)} = 0$ center could be envisioned if a Jahn−Teller distortion of the d^4 orbitals resulted in two of the t_{2g} orbitals being lower in energy, leaving the third unoccupied.[35] As a consequence of deprotonation of the aquo ligands, this species exhibits both optical[20] and EPR[26] spectral changes as a function of pH. In the EPR spectrum, the maximum shifts to a higher g-value with increasing pH. As expected, there is no EPR signal detected from the {4,4} species. However, a broad rhombic signal centered near $g \approx 1.98$ can be assigned to the {4,5} intermediate, also characteristic of an $S = 1/2$ system (Figure 1B).[22]

Unlike PSII, in which the S_4 state is difficult to trap, the blue dimer can be routinely isolated in the {5,5} state because of the 10^4-fold slower turnover rate.[8−10] This form has been characterized by RR, electronic absorption spectroscopy, cyclic voltammetry (CV), and differential pulse polarography, results from which all are consistent with a $(O)Ru^V-O-Ru^V(O)$ core.[8−10,36] Distorted octahedral d^3 Ru centers will exhibit an $S_{Ru(V)} = 3/2$ or $S_{Ru(V)} = 1/2$ ground state if the unsymmetric ligand field and the characteristically large spin orbit coupling ($0.13 − 0.14$ eV) removes the degeneracy of the t_{2g} orbitals.[24] In both cases a strongly antiferromagnetically coupled Ru^V-O-Ru^V intermediate would result in an $S = 0$ ground state, generating an EPR silent species. Nonetheless, solutions containing {5,5} display a near-axial $g \approx 2$ signal (Figure 1C) indicating the presence of unpaired spin(s). Under photocatalytic conditions, rate of decay of the $g \approx 2$ signal parallels the decline in the rate of oxygen evolution after the illumination source has been removed, suggesting that this paramagnetic species is an integral part of the catalytic cycle.[36,39] This $g \approx 2$ signal is the focus of this paper.[8,10,36] Appearance of this signal is at odds with the formal description of the {5,5} species as having a $(O)Ru^V-O-Ru^V(O)$ core which, assuming significant Ru−Ru spin-coupling across the bridging oxo atom, should be EPR-silent. More reasonably, this EPR signal can be assigned to a species with an odd electron system such as a molecule with a Ru^V-O-Ru^{IV} core, unique from the {4,5} species in Figure 1B since this species is not observed below pH 2. Fortunately, EPR spectroscopy allows us to probe specific species on a background that will contain multiple intermediates, some of which will be paramagnetic. The assigned formulations (Ru oxidation states, protonation states, magnetic structures) for each of the species involved are summarized in Supporting Information, Table S1.

Herein, we report the first advanced EPR studies on the near-axial $g \approx 2$ signal associated with the catalytically active solutions in which the {5,5} complex is present. The $^{99,101}Ru$ hyperfine couplings of the $g \approx 2$ signal were characterized by continuous wave (CW) EPR methods, while much smaller ^{14}N hyperfine couplings originating from the bipyridine ligands were monitored by electron spin echo envelope modulation (ESEEM) and hyperfine sublevel correlation spectroscopy (HYSCORE). To identify any solvent or chemically exchangeable protons $^1H/^2H$ electron nuclear double-resonance (ENDOR) was employed. These spectroscopic findings are analyzed to provide possible electronic structure descriptions for the {5,5}-derived intermediate.[8]

EXPERIMENTAL SECTION

Materials. The complex ion $[Ru(bpy)_2(OH_2)]_2O^{4+}$ was isolated as its perchlorate salt.[22] Spectrochemical titrations of {3,3} with Ce^{4+} in trifluoromethanesulfonic (triflic) acid, CF_3SO_3H, yielded clean isosbestic points, confirming the purity of the {3,3} starting material.[21,22] CF_3SO_3H was twice-distilled under reduced pressure and stored at 4 °C as a 2 M solution. Other reagents were best-available grade from commercial suppliers and were used as received. House-deionized water was further purified using a reverse osmosis-deionization system. The higher oxidation states of {3,3} were generally prepared by constant potential electrolysis (CPE) using a carbon fiber electrolysis flow cell (Model HX-201, Hokuto Denko (Tokyo)) with a surface area of ≈ 3000 cm² and a working volume of 2 mL.[21] The cell was controlled by an EG&G-PAR model 273 potentiostat/galvanostat whose applied potentials were referenced against a Ag/AgCl electrode. Some of the samples used for the EPR studies were instead oxidized by $Ce^{IV}(CF_3SO_3)_4$ or Co^{III}.[41] No

differences in the EPR spectra were observed when the complex was oxidized by these methods.

EPR Spectroscopy. All EPR experiments at the X- and Q-band were carried out at the CalEPR facility at UC Davis. Low-temperature X-band (9 GHz) EPR spectra were collected using either a Bruker model ECS106 or E500 (Bruker BioSpin, Billerica, MA) equipped with a Bruker SHQ or TE102 (ER4102ST) resonator and an EIP 548A frequency counter. All CW spectra at X-band frequencies were collected at temperatures between 10−40 K under nonsaturating, slow-passage conditions. Temperature was maintained with an Oxford Instruments model ESR900 helium flow cryostat with an Oxford ITC 503 temperature controller. Pulse EPR spectra collected at Q-band (34 GHz) frequencies were acquired with a Bruker Elexsys E580 pulse EPR spectrometer (Bruker BioSpin, Billerica, MA) using an EN 5107D2 Q-band EPR/ENDOR probe and a laboratory-built TE_{011} brass cavity and coupler following a standard design.[42,43] Temperature control was achieved with an Oxford ITC 503 temperature controller. All Q-band spectra were acquired at 10 K. Electron spin echo (ESE)-detected ENDOR was performed using the Davies ENDOR sequence, with stochastic data collection.[44,45] All parameters are listed in the respective figure captions. All EPR spectral simulations were performed within the Matlab 7.5.0.342 (R2007b) software package (The Mathworks Inc., Natick, MA) using the EasySpin 4.0.0 toolbox.[46,47]

■ RESULTS

Characterization of the CW EPR Spectrum. The EPR spectrum corresponding to solutions containing the {5,5} intermediate (Figure 2) exhibits a near-axial signal with effective
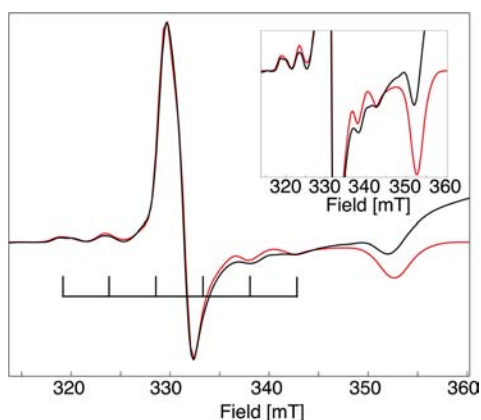
Figure 2. 9.371 GHz CW EPR spectrum (black) in {5,5}-containing solutions. Spectrometer setting: temperature = 40 K; modulation amplitude = 8 mT; modulation frequency = 100 kHz; microwave power = 6.32 mW. Simulation parameters: $S = 1/2$; $g = [2.033\ 2.020\ 1.899]$; $A(^{99/101}Ru) = [130\ 40\ 30]$ MHz; $Apa = [0\ 0\ 40]*\ \pi\ /180$; line width = 1.3 mT. Simulations (red) include both nuclear magnetic isotopes (^{99}Ru, $I = 5/2$, $\gamma = 1.954$, 12.76% abundance and ^{101}Ru, $I = 5/2$, $\gamma = 2.193$, 17.06% abundance; I is the nuclear spin, γ is the gyromagnetic ratio) as well as nonmagnetic isotopes. Inset: Expanded view of the region displaying $^{99,101}Ru$ hyperfine coupling.

g-values of $g_\perp = 2.03$ and $g_\| = 1.89$, identical to previous reports.[8,36] Because of a significant proportion of the complex adsorbing to the CPE flow cell, all spin quantitation studies were performed on samples oxidized chemically with $Ce^{IV}(CF_3SO_3)_4$. By comparing the doubly integrated spectrum of the $g \approx 2$ signal to that for a series of $CuSO_4$ standards (collected under nonsaturating conditions) we estimate that 5% of total $[Ru_2]$ in the sample is responsible for the EPR signal (it is important to note that spin quantitation has an uncertainty of about 10−20%).[48] A two-dimensional phase-inverted echo-

amplitude detected nutation (PEANUT) experiment was employed to confirm the $S = 1/2$ spin of the species responsible for the $g \approx 2$ signal present during water oxidation.[49] This experiment untangles different spin systems by correlating the nutation frequency with the resonant field, revealing information on mixtures and types of spin states.[49] The PEANUT experimental result shows that the signal from {5,5}-containing solutions is composed of only one type of Kramers spin system with a nutation frequency of ≈8 MHz (Supporting Information, Figure S1), almost identical to that of the tyrosine radical Y_D in PSII (a known $S = 1/2$ species, Supporting Information, Figure S2) which we measured under identical spectrometer conditions.

Six evenly spaced peaks centered about the principal resonance at $g_\perp$ are resolved in the CW EPR spectrum (Figure 2). These peaks are attributed to hyperfine coupling of the unpaired electron with at least one Ru nucleus and account for ≈30% of the integrated signal intensity, as revealed by simulations including all of the Ru isotopologues. The two magnetic isotopes of ruthenium together have 29.8% natural abundance (^{99}Ru, $I = 5/2$, $\gamma = 1.954$, 12.76% abundance and ^{101}Ru, $I = 5/2$, $\gamma = 2.193$, 17.06% abundance; I is the nuclear spin, γ is the gyromagnetic ratio). The unpaired spin of each Ru center appears to be highly localized, a result of little if any Heisenberg exchange between the metal sites (a class I type exchange interaction) indicated by the six hyperfine lines ($2I + 1$, $I = 5/2$) in the spectrum in Figure 2. This is in contrast to a delocalized spin, which occurs in more strongly coupled systems (Robin and Day class II, and III).[50] Very strong exchange coupled systems are defined as Class III and would result in the unpaired electron being equally shared between both metal centers, yielding an eleven-peak splitting pattern in the EPR spectrum (e.g., the copper A centers in cytochrome c oxidase and nitrite reductase).[51,52] Multinuclear clusters, such as Mn dimers (^{55}Mn, $I = 5/2$, 100% abundance; same nuclear spin as ^{99}Ru and ^{101}Ru) commonly exhibit intermediate class II exchange interactions which typically arise from antiferromagnetic coupling, resulting in "multiline"-type spectra where 12−18 peaks are observed.[53] If the unpaired electron were delocalized in the "blue dimer", the "multiline" feature would have reduced intensity because of the low magnetic isotope abundance of the Ru ions (i.e., 30% × 30% = 9% integrated signal intensity). This multiline feature would be observed overlaid upon the already resolved six peaks. However, extensive signal averaging did not reveal any additional satellite lines (Supporting Information, Figure S4). Additionally, if both Ru centers were equally coupled to the unpaired electron the six primary metal hyperfine peaks would have double the amplitude relative to the parent peak at $g \approx 2$. Ruthenium hyperfine values of $[130 \pm 5, 40 \pm 10, 30 \pm 10]$ MHz are needed to fit these satellite lines. These hyperfine values are relatively large compared to a number of other ruthenium complexes, particularly those containing multidentate ligand-centered radicals, which typically exhibit hyperfine coupling constants in the range of 0 to 60 MHz (Supporting Information, Table S2).[30,54−59] Thus the comparatively large ^{99}Ru and ^{101}Ru hyperfine observed for the $g \approx 2$ signal is consistent with localization of a significant amount of spin density on the metal center rather than on the bipyridine ligand(s). Density functional theory computations have also suggested that progressive oxidation from {3,3} to {5,5} occurs with loss of electron density primarily in the bipyridine ligands, rather than the dinuclear core.[36]
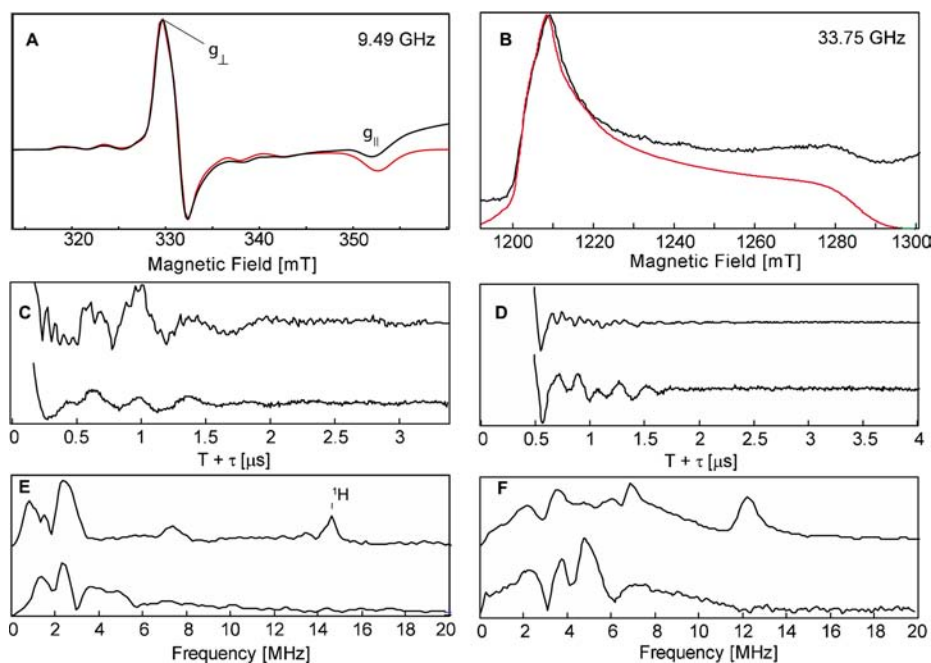
Figure 3. EPR spectra of {5,5} solutions collected at X-band (3A) and Q-band (3B) frequencies. Top panels are the CW (9.37 GHz) and echo detected (33.75 GHz) field-swept spectra (black) with simulations (red). Simulation parameters are reported in Figure 2. Figure 3C and 3D are the time domain ESEEM data with the corresponding cross-term averaged Fourier transform frequency domain (3E and 3F).[47] The top spectrum in each figure is collected on resonance with $g_\perp$, and the bottom spectrum is in resonance with $g_\parallel$.
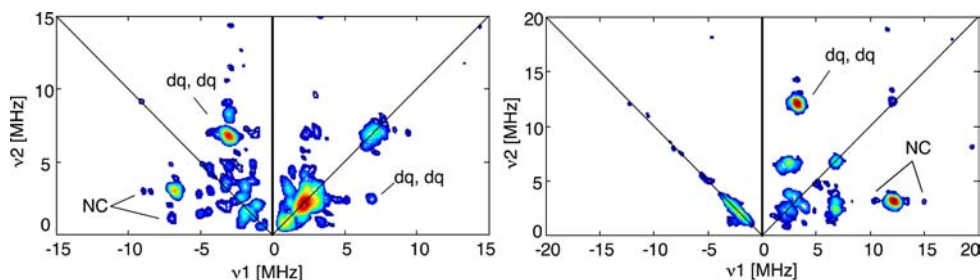
Figure 4. X-band HYSCORE spectrum of {5,5} solutions on the left and the corresponding Q-band HYSCORE spectra on the right. Both spectra are acquired on resonance with $g_\perp$. Spectrometer setting: temperature = 20 K; $t(\pi/2)$ = 24 ns; tau (τ) = 132 ns; microwave power = 0.635 mW. NC indicates the multinuclear coherence frequencies.

The analysis of the CW EPR results presented above point to the signal from {5,5}-containing solutions as arising from at least one Ru center with a total $S = 1/2$ spin. A possible electronic structure description that could explain these results is a single unpaired spin localized at one of the Ru═O units suggesting that the observed species is at least one electron reduced from a formal {5,5} oxidation state. In this case, the paramagnetic moiety could be described as a Ru^{IV} center with a $S_{Ru(IV)} = 0$ bound, through an oxo bridge, to a Ru^V═O. In the following sections, we describe results from a variety of advanced EPR studies designed to probe the ligand environment about these ruthenium ions to further support these oxidation state assignments.

ESEEM and HYSCORE of the ^{14}N Ligand Contributions. To obtain more detailed information about the spin density distribution about the molecule, we employed advanced pulse EPR techniques including three-pulse ESEEM and HYSCORE spectroscopies to probe the electron spin density at the nitrogen atoms found in the bipyridine ligands. The nuclear spin flip frequencies determined from these experiments can reveal information about the hyperfine couplings and

quadrupole interactions from the $I \geq 1$ nuclei (e.g., ^{14}N). Optimal ESEEM spectra are achieved when the cancellation condition is met where the isotropic hyperfine interaction (A_{iso}) cancels any contributions in the nuclear Zeeman manifold, resulting in pure nuclear quadrupole (NQ) states in the corresponding manifold.[60] These NQ frequencies, ν_0, ν_-, and ν_+ are revealed by Fourier transform of the ESEEM spectrum and can give information on the electric field gradient across the nucleus described by e^2qQ/h and the asymmetry parameter η, which ranges from 0, axial, to 1, rhombic.[60] These values report on the symmetry of the electronic charge distribution about the nucleus and thus can disclose the type of nitrogen and its protonation state. These frequencies can appear in the ESEEM spectrum as narrow peaks; as these conditions deviate from the cancellation limit, the peaks can broaden or become completely absent.[60] In the opposite electron spin manifold, the isotropic hyperfine and the Zeeman interactions are additive resulting in three additional transitions, two of which are so-called single-quantum transitions (ν_{sq}) and the double quantum transition (ν_{dq}). While the frequencies of the ν_{sq} transitions are not always resolved in the ESEEM spectrum, the isotropic

hyperfine coupling can still be determined from the double quantum transition, assuming the anisotropic component is small.[61]

$$|A_{iso}| = \frac{\nu_{dq,a}^2 - \nu_{dq,b}^2}{8\nu_I} \tag{1}$$

The three-pulse ESEEM spectrum of the $g \approx 2$ signal was obtained at multiple frequencies. The time-domain spectra and the corresponding cross-term averaged Fourier transform frequency spectra are presented in Figures 3E and 3F.[47] The X-band ESEEM spectrum acquired on resonance with $g_\perp$ reveals peaks at 1.0, 2.4, 6.9, and 15 MHz. The associated spectrum on resonance with $g_\parallel$ has peaks at 1.4 and 2.3 MHz. The peak at 15 MHz arises from weakly coupled protons. The Q-band ESEEM spectrum collected in resonance with $g_\perp$ has peaks at 2.3, 3.6, 4.9, 6.1, 6.8, and 12.2 MHz. The corresponding $g_\parallel$ spectrum has peaks at 2.3, 3.8, 4.8, 7.5 MHz.

HYSCORE spectroscopy separates features from multiple hyperfine coupled atoms that might be overlapping in the one-dimensional ESEEM spectra. This is important for the "blue dimer" since there are eight nitrogen atoms on each dimer. Nitrogen atoms that could give rise to appreciable hyperfine couplings can be further classified those being axially or equatorially bound. The X-band HYSCORE spectrum (Figure 4, left) has $\nu_{dq,a} - \nu_{dq,b}$ cross peaks in the + + quadrant at (3.3, 1.1) and (2.5, 6.9) MHz, and in the + − quadrant at (6.8, 3.0) MHz. The shift of peaks to the + − quadrant in the X-band spectrum is characteristic of strong or intermediate coupling ($A > 2\nu_I$ or $A \approx 2\nu_I$, respectively) and opposite signs for nuclear coherent frequencies.[62] Cross peaks assigned to the $\nu_{dq,a} - \nu_{dq,b}$ transition frequencies in the Q-band HYSCORE spectrum are observed in the + + quadrant at (3.0–3.5, 12.0–12.5); (1.8–2.5, 6.7–6.9) and (2.7, 3.8) MHz (Figure 4, right). Three different classes of nitrogen hyperfine couplings can be assigned from the $\nu_{dq,a} - \nu_{dq,b}$ peaks observed in the X- and Q-band HYSCORE spectra. The $\nu_{dq,a} - \nu_{dq,b}$ cross-peaks will shift by twice the difference of the Larmor frequency (ν_I) for the respective X- and Q-band fields. Therefore, the $\nu_{dq} - \nu_{dq}$ cross-peaks in the + + quadrant of the X-band HYSCORE can be assigned to the same two classes of nuclei that give rise to the $\nu_{dq,a} - \nu_{dq,b}$ peaks in the + + quadrant of the Q-band HYSCORE. An additional set of cross peaks in the + − quadrant of the X-band HYSCORE can be assigned to a unique class of nitrogen atoms. Using eq 1, and the positions of the $\nu_{dq} - \nu_{dq}$ cross-peaks in both the X- and Q-band HYSCORE spectra, we compute three classes of nitrogen A_{iso} couplings: 1.2 ± 0.2, 4.25 ± 0.25 and 4.85 ± 0.55 MHz.

Additional peaks at (3, 8.3) and (2.1, 7.1) MHz in the + − quadrant of the X-band spectrum and (3.2, 14.5) and (3.2, 10.5) MHz in the + + quadrant of the Q-band spectrum are diagnostic of multinuclear coherences (NC).[63] These additional peaks indicate that the strongly hyperfine-coupled ^{14}N nuclei are part of the same spin system as another nucleus with nuclear spin-flip transition frequencies of (1.4, 4.4) and (1.1, 3.2) MHz for the X-band spectrum and (2.5, 4.0) and (1.5, 2.7) MHz in the Q-band spectrum.

[1]H/^{2}H ENDOR. ENDOR experiments were performed on solutions of {**3,3**} oxidized in 0.1 M TFA in 100% H_2O or 95% D_2O to detect any solvent or chemically exchangeable ligand protons in the vicinity of the paramagnetic Ru center. Q-band Davies and Mims ENDOR spectra of {**5,5**} solutions were collected at 1205.6 mT which is on-resonance with $g_\perp$. The ENDOR spectrum of the "blue dimer" oxidized in ^{1}H TFA

possesses four sets of peaks centered at the [1]H Larmor frequency (ν_L = 51.3 MHz at 1205.6 mT) and split by 7.4, 5.6, 2.5, and 1.0 MHz (Figure 5). All these features are present in
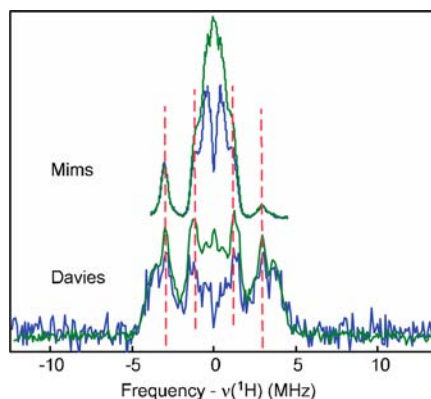
Figure 5. [1]H/^{2}H ENDOR at Q-band microwave frequencies (34 GHz) of {**5,5**} solutions oxidized in 0.1 M TFA 100% H_2O (green) and 95% D_2O (blue). Top: Mims, Bottom: Davies. Spectrometer setting: temperature = 10 K; $t(\pi/2)$ = 44–92 ns, tau (τ) = 200–400 ns; RF = 36 μs.

the spectrum of the sample oxidized in ^{2}H TFA; however, the intensity of the innermost sets of peaks decreases somewhat. These features represent protons with rather small effective hyperfine couplings, suggesting the proton is removed from the spin center leading to weak hyperfine couplings to the unpaired spin density or solvent protons not coordinating the dimer, also know as "matrix" protons.[64] Mims ENDOR, which is better suited for detecting more weakly hyperfine-coupled nuclei, was also performed to probe the exchangeable protons. The Mims ENDOR spectrum collected on-resonance with $g_\perp$ (1205.6 mT) revealed four sets of features centered at the [1]H Larmor frequency and split by 5.97, 2.08, 1.13, and 0.75 MHz, respectively. The set with the largest observed splitting in the Davies ENDOR spectrum is not resolved in Mims ENDOR because of Mims holes that appear at 4 and 2 MHz.[64,65]

While no change in intensity was observed for peaks with the largest splitting in the Davis ENDOR spectrum, the difference between the ^{1}H and [2]H Mims spectra results in a featureless peak with a width of about 1 MHz, which could be consistent with matrix protons in solution or a very distant ligated proton that is solvent exchangeable. In summary, it is clear that the observed peaks with splittings of 7.4 and 6.2 MHz correspond to more strongly coupled protons that are not exchanging with solvent deuterons during the course of the experiment. We can simulate these protons with two classes of strong hyperfine couplings A_{H1} = 7 MHz and A_{H2} = 6 MHz. There is an additional class of weakly coupled protons with A_{H3} = 2.5 MHz (Supporting Information, Figure S5). These protons could be found in the bipyridine ligands.

Modifications to the Bipyridine Ligands. Finally, CW EPR studies were carried out on analogous Ru dimers whose bipyridine ligands bear weakly electron-donating substituents, that is, 4,4′- and 5,5′-dimethyl-2,2′-bipyridine (DMB), to determine how modifications to the ligand affected the $g \approx 2$ EPR spectrum. All solutions were oxidized with 20 equiv of $Ce^{IV}(CF_3SO_3)_4$ to convert the complex completely to the {**5,5**} state. All three spectra are nearly identical with the only distinctions being slight shifts in the observed g-values for the respective spectra (Supporting Information, Figure S8). The

complex that shows the most deviation from the EPR spectral properties of the underivatized sample was the 4,4′-DMB complex. Because of the electron donating nature of the methyl groups and their close proximity to the metal centers, enhanced spin density could be pushed onto the Ru ions, leading to a larger shift in the g-values in the 4,4′-DMB complex. However, no significant changes to the line shape of the EPR spectra were observed. This lack of significant spectral change would seem to rule out hydroxylation of the unsubstituted bipyridine ligands at either the 4′ or the 5′ positions.

■ DISCUSSION

Identity of the $g \approx 2$ Species. Electrochemical (1.55 V vs Ag/AgCl) or chemical ($Ce^{IV}(CF_3SO_3)_4$) oxidation of {3,3} to {5,5} affords a transiently stable paramagnetic species characterized by a nearly axial EPR spectrum ($g = [2.033\ 2.020\ 1.899]$; Figures 1, 2;).[8,10,36] We see no way that two $Ru^V=O$ moieties can reside on the same molecule and give rise to this signal since such a species would be expected to be either EPR silent (e.g., if two $S = 1/2$ sites coupled antiferromagnetically to yield a net $S = 0$ spin system) or give rise to a prototypical triplet spectrum if the two spin centers were weakly coupled either ferromagnetically or through space.[66] Using the crystallographically determined internuclear distances, the predicted dipolar coupling between two $Ru^V=O$, where the bulk of spin density is carried by the metal center, is estimated to be on the order of ≈800 MHz.[20,67] Such dramatic splitting of the EPR signal is not observed (Figure 2); therefore, we can rule out the axial $g \approx 2$ spectrum as arising from an ion whose electronic structure corresponds to $(O)Ru^V-O-Ru^V(O)$. Instead, what we detect could arise from a mixed-valence species, such as a unique $Ru^{IV}-O-Ru^V$ ($S_{Ru(V)} = 1/2$; $S_{Ru(IV)} = 0$) species formed upon reaction of {5,5} with water as part of the overall oxidation process. The six-line hyperfine splitting pattern resolved in the X-band CW spectrum indicates that the unpaired spin primarily resides on only one of the Ru ions. Simulations of the X-band CW spectra reveal a splitting pattern that would suggest there is only one Ru ion with unpaired spin density supporting this conclusion.

The other reasonable possibility is that the $g \approx 2$ signal arises from a form of a unique $Ru^{IV}-O-Ru^V$ species whose electronic structure is best represented as $(OH)Ru^{IV}-O-Ru^{IV}(O^{\bullet})$. Radicaloid species such as these have previously been proposed by Yang and Baik on the basis of density functional theory (DFT) calculations to be an appropriate description of the actual electron distribution in {5,5}.[68] Oxyl radical species of this type have much presence in the literature in both Ru complexes as well as Mn complexes invoked as models for Mn_4Ca cluster in PSII that is also involved in oxygen evolution.[68−73] This configuration also closely mimics the electronic structure of a Fe^V-TAML complex that was confirmed to be a low spin $S = 1/2$ system.[74]

The modest g-shifts observed for the $g \approx 2$ signal in Figure 2, can also reasonably be explained by an $(OH)Ru^{IV}-O-Ru^{IV}(O^{\bullet})$ electronic configuration. For more metal-centered radicals, a larger degree of g-anisotropy is expected.[75−77] The Ru^V center has a $(t_{2g})^3$ electron configuration because Dq is quite large for Ru. Including the oxo group electrons gives us the qualitative molecular orbital diagram shown below in Figure 6. That $\Delta g_{\parallel} = 0.10$ indicates that the Ru−O π* ligand-field states are separated by 30 000 cm⁻¹ if the unpaired electron is wholly on the ruthenium ion ($x_{Ru} = 1500$ cm⁻¹). This large gap would suggest a significant, and perhaps unrealistic, Jahn−
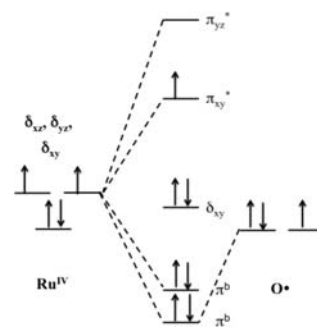
Figure 6. Molecular orbitals involving the Ru d electrons in a $Ru^{IV}-O^{\bullet}$ configuration.

Teller-induced elongation of the Ru−N bond trans to the oxo-group leading to stabilization of one of the π* orbitals. Alternatively, if the spin is delocalized onto the oxo ligand, effectively giving $Ru^{IV}-O^{\bullet}$, then the gap could be as little as 3000 cm⁻¹ (assuming 70% oxyl character as predicted by some DFT results[68]). Furthermore, an $A_{iso}(^{99/101}Ru) \approx 100$ MHz indicates that the magnetic orbital has 6% Ru s-character, suggesting a significant portion of the unpaired spin density could be located on the oxo ligands.

Assuming that the $g \approx 2$ signal is attributable to a $(OH)Ru^{IV}-O-Ru^{IV}(O^{\bullet})$ radicaloid form of the "blue dimer", the spin quantitation measurements indicate that this species constitutes only a few percent of the total ruthenium concentration, at liquid He temperatures. Presumably, then, the remainder is in the strongly coupled EPR-silent $(O)Ru^V-O-Ru^V(O)$ form. As such, this interpretation implies the existence of two discrete chemical entities at this level of oxidation. Based upon the proportionate loss of the $g \approx 2$ signal and total amount of {5,5} in photoexcitation experiments,[39] these entities would have to be in rapid equilibrium with each other.

Both the {4,5} (Figure 1B) and {3,4} (Figure 1A) species have a total $S = 1/2$ spin and could in principle account for the $g \approx 2$ EPR signal appearing in {5,5}-containing solutions. However, the {4,5} intermediate is not stable below pH 2 and has a distinct EPR spectrum (Figure 1B).[22] The {3,4} oxidation state is very stable, but also has a distinct EPR spectrum (Figure 1A). Therefore, neither {3,4} nor {4,5} can be responsible for the axial $g \approx 2$ spectrum that we observe here. While there are only limited EPR data reported for d³ Ru^V monomeric complexes, the CW EPR spectra are understood in terms of a $S = 1/2$ ground state.[59,78] Therefore, it is conceivable that the EPR signal might arise from a decomposition product such as a low-spin mononuclear Ru^V-containing fragment of the "blue dimer". However, it is quite evident from RR and mass spectrometric studies that the Ru−O−Ru bond is retained following repeated cycling of the catalyst, confirming that the complex remains dimeric, ruling out monomer accumulation as the source of the signal.[22,36,79] Alternatively, the EPR signal could arise from an overoxidized {5,6} complex. However, previous results utilizing flow-CPE to explore the composition of dimer solutions as a function of applied potential indicated that the amplitude of the signal was independent of potentials above those required to quantitatively oxidize the complex to {5,5} (1.6 V vs NHE).[21] These EPR/potentiometric analyses were repeated in this study, confirming this behavior. These data are inconsistent with the further oxidation of an EPR-silent {5,5} ($S = 0$) to an $S = 1/2$ {5,6} ion, the thermodynamic

potential for which must be above 1.6 V, and which therefore would increase in concentration as the applied potential was increased.

It is important to also note that the $g \approx 2$ signal under investigation here is not seen in highly oxidized acidic solutions containing high concentrations of nitrate ion. Instead, a broad rhombic signal reminiscent of {3,4} appears whose g-value is shifted to lower fields.[32] The appearance of this signal coincides with dramatic changes in the RR spectra of the dimer that comprise loss of the characteristic Ru=O vibrational bands of {5,5}, the appearance of a new (as yet unassigned) O-isotope-sensitive band at ≈ 680 cm^{-1}, and changes in frequencies and intensities of the Ru−O−Ru symmetric stretching mode region; these changes indicate that extensive modifications of the chemical structure of the dimer have occurred.[21,32] In a recent analysis that included X-ray absorption spectroscopic measurements, Pushkar and associates suggested that the new species was a {3,4} ion containing a peroxo ligand, which they denoted as [3,4]′;[32] although reasonable, the evidence presented in support of this assignment is not definitive. At very early times (≤ 10 s), an additional signal appears whose features are similar to the {4,5} signal reported here (Figure 1B), but apparently arise from a distinct species at this level of oxidation since this signal is generated in strongly acidic solutions where {4,5} disproportionates.[22,26,32] Our own research points to an alternative nitrate-dependent reaction pathway as the origin of [3,4]′. These studies have been reported separately, but are mentioned here to avoid confusion; our samples are prepared under conditions where these complicating features are avoided.[41]

Is the $g \approx 2$ Signal from a Complex Containing a Bipyridine Radical? Based upon its relatively narrow bandwidth and low rhombicity, the $g \approx 2$ signal previously was tentatively assigned to a bipyridine ligand radical-containing reaction intermediate.[10,36] It was further postulated that this species might be a {4,5} ion containing a hydroxylated bipyridine formed by concerted addition of the elements of water to {5,5}. Indeed, evidence for formation of this type of intermediate during catalytic cycling of the "blue dimer" has been obtained in the form of NIR optical spectra in photocatalyzed reactions,[39] pulse radiolysis experiments that characterize "blue dimer"−OH adducts,[36] and theoretical studies that establish the plausibility of this reaction in bipyridine complexes containing highly oxidized Ru centers.[80] However, it is unclear how the unpaired spins on the metal center and ligand would interact in such a species (e.g., {4,5}-bpyOH$^\bullet$) and, more pointedly, we do not observe any ^{1}H or ^{14}N hyperfine contributions that would be indicative of a bipyridyl radical, refer to Figure 7 for the assigned coupling constants. Further, that the {5,5} containing solutions for functionalized bipyridine ligands gives essentially the same EPR spectrum would seem to preclude bipyridine hydroxylation.

ARu = [140, 30, 40] MHz;
AH$_1$ = 2.5 MHz; AH$_2$ = 6 MHz; AH$_3$ = 7 MHz;
AN$_1$ = 1.2 ± 0.2 MHz; AN$_2$ = 4.25 ± 0.25 MHz;
AN$_3$ = 4.85 ± 0.55 MHz
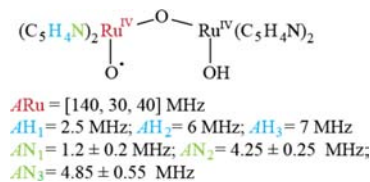
Figure 7. Scheme detailing the hyperfine coupling interactions determined from our EPR studies.

Nonetheless, our results can only confirm the observed $g = 2$ EPR signal is likely not associated with an intermediate that has been hydroxylated and does not exclude a hydroxylated species or a bipyridine ligand radical forming at a distinct point in the mechanism.

The present study clearly assigns a large hyperfine coupling to the Ru ions, which is also inconsistent with a bipyridine ligand-centered radical. Support for this assignment is based on analysis of the multifrequency ESEEM, HYSCORE, and ENDOR data. We find a maximum ^{14}N hyperfine coupling ≈ 5.4 MHz. The relatively small magnitude of the hyperfine coupling is most consistent with the bipyridine nitrogen atoms coordinated to the paramagnetic metal center. Typical ^{14}N hyperfine couplings for ruthenium complexes with an unpaired spin found localized primarily on the ligand such as bipyridine fall in the range of 7−22 MHz (Supporting Information, Table S2).[30,54,57,58] Conversely, measurements probing the ^{14}N hyperfine coupling of nitrogen containing ligands in a Mn^{III}Mn^{IV} bipyridyl dimer reveal ^{14}N hyperfine couplings in the range of 2.78−11.4 MHz (see ref 81 and references therein).[81] Furthermore, a hyperfine coupling of 5.5 MHz has been measured for an electrophilic low spin Ru^{III} nitrido complex.[82] The ^{14}N hyperfine coupling measured for solutions containing the {5,5} state of the "blue dimer" is characteristic of a nitrogen-containing ligand (e.g., bipyridine) bound to a metal center. Furthermore, we can designate the hyperfine couplings ranging between 4.0−5.4 MHz to the equatorial ligands as there would be little to no spin density in the orbitals bound to the axially coordinated nitrogen atoms. These more weakly coupled nuclei can reasonably be assigned to the nitrogen hyperfine couplings between 1.0−1.4 MHz. It is important to note however, that this does not exclude the possibility of a ligand-centered radical also being an undetected transient species, as has been suggested in previously proposed pathways.[39,79]

The ^{1}H hyperfine coupling revealed by ENDOR experiments of the nonexchangeable protons are likely derived from the bipyridine ligands. For comparison, ^{1}H ENDOR on the Fe$_4$S$_4$ cluster found in carbon monoxide dehydrogenase revealed exchangeable proton couplings on the order of 6−15 MHz.[83] These protons were assigned to a terminal ligand or hydrogen-bonded protons in the cluster sulfur atoms.[83] ENDOR studies carried out on a number of Mn^{III}Mn^{IV} dimers revealed hyperfine couplings from 1.2−19.8 MHz. These proton hyperfine couplings were all assigned to ligand derived contributions.[53,84] The exchangeable protons, on the other hand, are likely due to matrix protons found in solution. However, we cannot exclude an exchanging hydroxyl group bound to the Ru^{IV} metal center.[8,80]

CONCLUDING COMMENTS

Our EPR analyses clearly show that the $g \approx 2$ signal observed in catalytically active solutions is attributable to an $S = 1/2$ species. The large Ru centered metal hyperfine couplings observed in the $g \approx 2$ signal exclude the assignment of the signal to a bipyridine-ligand centered radical. ESEEM, HYSCORE, and ENDOR spectroscopic studies probing the ^{1}H and ^{14}N ligand contributions are consistent with neutral bipyridine groups bound to a metal center. Furthermore, the relatively large Ru hyperfine interaction points to significant metal character in the magnetic orbital. An odd electron system with $S = 1/2$, such as a molecule with a Ru^V−O−Ru^{IV} core or an intermediate with a Ru−O$^\bullet$ oxyl radical moiety coupled to a Ru^{IV} species, would be

consistent with this formulation. The ruthenyl-oxyl radical species assignment is preferred because of the relatively small g-anisotropy observed in the CW EPR spectrum. As oxygen has a much smaller spin−orbit coupling constant than does ruthenium, the more spin delocalized on this nucleus would lead to small g-shifts.

■ ASSOCIATED CONTENT

Ⓢ Supporting Information

Further details are given in Tables S1−S2 and Figures S1−S8. This material is available free of charge via the Internet at http://pubs.acs.org.

■ AUTHOR INFORMATION

Corresponding Author

*E-mail: rdbritt@ucdavis.edu.

Notes

The authors declare no competing financial interest.

■ ACKNOWLEDGMENTS

■ REFERENCES

(1) Bard, A. J.; Fox, M. A. *Acc. Chem. Res.* **1995**, *28*, 141.
(2) Kanan, M. W.; Surendranath, Y.; Nocera, D. G. *Chem. Soc. Rev.* **2009**, *38*, 109.
(3) Barber, J. *Phil. Trans. R. Soc., A* **2007**, *365*, 1007.
(4) Eisenberg, R.; Gray, H. B. *Inorg. Chem.* **2008**, *47*, 1697.
(5) Dau, H.; Zaharieva, I.; Haumann, M. *Curr. Opin. Chem. Biol.* **2012**, *16*, 3.
(6) Williamson, A.; Conlan, B.; Hillier, W.; Wydrzynski, T. *Photosynth. Res.* **2011**, *107*, 71.
(7) Grundmeier, A.; Dau, H. *Biochim. Biophys. Acta, Bioenerg.* **2012**, *1817*, 88.
(8) Clark, A. E.; Hurst, J. K. *Prog. Inorg. Chem.* **2011**, *1*, 1.
(9) Liu, F.; Concepcion, J. J.; Jurss, J. W.; Cardolaccia, T.; Templeton, J. L.; Meyer, T. J. *Inorg. Chem.* **2008**, *47*, 1727.
(10) Hurst, J. K. *Coord. Chem. Rev.* **2005**, *249*, 313.
(11) Dismukes, G. C.; Brimblecombe, R.; Felton, G. A. N.; Pryadun, R. S.; Sheats, J. E.; Spiccia, L.; Swiegers, G. F. *Acc. Chem. Res.* **2009**, *42*, 1935.
(12) Yamazaki, H.; Shouji, A.; Kajita, M.; Yagi, M. *Coord. Chem. Rev.* **2010**, *254*, 2483.
(13) Das, B. K.; Chakrabarty, R. *J. Chem. Sci. (Bangalore, India)* **2011**, *123*, 163.
(14) Najafpour, M. M.; Rahimi, F.; Aro, E.-M.; Lee, C.-H.; Allakhverdiev, S. I. *J. R. Soc. Interface* **2012**, *9*, 2383.
(15) Wiechen, M.; Berends, H.-M.; Kurz, P. *Dalton Trans.* **2012**, *41*, 21.
(16) Tong, L. P.; Duan, L. L.; Xu, Y. H.; Privalov, T.; Sun, L. C. *Angew. Chem., Int. Ed.* **2011**, *50*, 445.
(17) Withers, N. *Nat Chem* **2010**.
(18) Surendranath, Y.; Dincă, M.; Nocera, D. G. *J. Am. Chem. Soc.* **2009**, *131*, 2615.
(19) Concepcion, J. J.; Jurss, J. W.; Templeton, J. L.; Meyer, T. J. *J. Am. Chem. Soc.* **2008**, *130*, 16462.

(20) Gilbert, J. A.; Eggleston, D. S.; Murphy, W. R.; Geselowitz, D. A.; Gersten, S. W.; Hodgson, D. J.; Meyer, T. J. *J. Am. Chem. Soc.* **1985**, *107*, 3855.
(21) Yamada, H.; Hurst, J. K. *J. Am. Chem. Soc.* **2000**, *122*, 5303.
(22) Cape, J. L.; Lymar, S. V.; Lightbody, T.; Hurst, J. K. *Inorg. Chem.* **2009**, *48*, 4400.
(23) Binstead, R. A.; Chronister, C. W.; Ni, J. F.; Hartshorn, C. M.; Meyer, T. J. *J. Am. Chem. Soc.* **2000**, *122*, 8464.
(24) Alperovich, I.; Smolentsev, G.; Moonshiram, D.; Jurss, J. W.; Concepcion, J. J.; Meyer, T. J.; Soldatov, A.; Pushkar, Y. *J. Am. Chem. Soc.* **2011**, *133*, 15786.
(25) Gersten, S. W.; Samuels, G. J.; Meyer, T. J. *J. Am. Chem. Soc.* **1982**, *104*, 4029.
(26) Lei, Y. B.; Hurst, J. K. *Inorg. Chem.* **1994**, *33*, 4460.
(27) Dobson, J. C.; Sullivan, B. P.; Doppelt, P.; Meyer, T. J. *Inorg. Chem.* **1988**, *27*, 3863.
(28) Patra, S.; Sarkar, B.; Mobin, S. M.; Kaim, W.; Lahiri, G. K. *Inorg. Chem.* **2003**, *42*, 6469.
(29) Yang, X. F.; Baik, M. H. *J. Am. Chem. Soc.* **2004**, *126*, 13222.
(30) Ye, S. F.; Sarkar, B.; Duboc, C.; Fiedler, J.; Kaim, W. *Inorg. Chem.* **2005**, *44*, 2843.
(31) Remenyi, C.; Kaupp, M. *J. Am. Chem. Soc.* **2005**, *127*, 11399.
(32) Moonshiram, D.; Jurss, J. W.; Concepcion, J. J.; Zakharova, T.; Alperovich, I.; Meyer, T. J.; Pushkar, Y. *J. Am. Chem. Soc.* **2012**, *134*, 4625.
(33) David, J.; Guerra, D.; Restrepo, A. *Inorg. Chem.* **2011**, *50*, 1480.
(34) Das, A.; Scherer, T. M.; Mobin, S. M.; Kaim, W.; Lahiri, G. K. *Inorg. Chem.* **2012**, *51*, 4390.
(35) David, J.; Guerra, D.; Restrepo, A. *Inorg. Chem.* **2011**, *50*, 1480.
(36) Hurst, J. K.; Cape, J. L.; Clark, A. E.; Das, S.; Qin, C. Y. *Inorg. Chem.* **2008**, *47*, 1753.
(37) Chronister, C. W.; Binstead, R. A.; Ni, J. F.; Meyer, T. J. *Inorg. Chem.* **1997**, *36*, 3814.
(38) Hurst, J. K.; Zhou, J. Z.; Lei, Y. B. *Inorg. Chem.* **1992**, *31*, 1010.
(39) Cape, J. L.; Hurst, J. K. *J. Am. Chem. Soc.* **2008**, *130*, 827.
(40) Okamoto, K.; Miyawaki, J.; Nagai, K.; Matsumura, D.; Nojima, A.; Yokoyama, T.; Kondoh, H.; Ohta, T. *Inorg. Chem.* **2003**, *42*, 8682.
(41) Stull, J. A.; Britt, R. D.; McHale, J. L.; Knorr, F. J.; Lymar, S. V.; Hurst, J. K. *J. Am. Chem. Soc.* **2012**, *134*, 19973.
(42) Sienkiewicz, A.; Smith, B. G.; Veselov, A.; Scholes, C. P. *Rev. Sci. Instrum.* **1996**, *67*, 2134.
(43) Calvo, R.; Abresch, E. C.; Bittl, R.; Feher, G.; Hofbauer, W.; Isaacson, R. A.; Lubitz, W.; Okamura, M. Y.; Paddock, M. L. *J. Am. Chem. Soc.* **2000**, *122*, 7327.
(44) Davies, E. R. *Phys. Lett. A* **1974**, *A 47*, 1.
(45) Epel, B.; Arieli, D.; Baute, D.; Goldfarb, D. *J. Magn. Reson.* **2003**, *164*, 78.
(46) Stoll, S.; Schweiger, A. *J. Magn. Reson.* **2006**, *178*, 42.
(47) Stoll, S.; Britt, R. D. *Phys. Chem. Chem. Phys.* **2009**, *11*, 6614.
(48) Hagen, W. R. *Dalton Trans.* **2006**, 4415.
(49) Stoll, S.; Jeschke, G.; Willer, M.; Schweiger, A. *J. Magn. Reson.* **1998**, *130*, 86.
(50) Bencini, A. G.; Gatteschi, D. *Electron Paramagnetic Resonance of Exchange Coupled Systems*; Springer Verlag: Berlin, Germany, 1990.
(51) Neese, F.; Kappl, R.; Huttermann, J.; Zumft, W. G.; Kroneck, P. M. H. *J. Biol. Inorg. Chem.* **1998**, *3*, 53.
(52) Neese, F.; Zumft, W. G.; Antholine, W. E.; Kroneck, P. M. H. *J. Am. Chem. Soc.* **1996**, *118*, 8692.
(53) Randall, D. W.; Chan, M. K.; Armstrong, W. H.; Britt, R. D. *Mol. Phys.* **1998**, *95*, 1283.
(54) Das, A. K.; Sarkar, B.; Fiedler, J.; Zalis, S.; Hartenbach, I.; Strobel, S.; Lahiri, G. K.; Kaim, W. *J. Am. Chem. Soc.* **2009**, *131*, 8895.
(55) Kaim, W.; Ernst, S.; Kasack, V. *J. Am. Chem. Soc.* **1990**, *112*, 173.
(56) Kaim, W.; Ernst, S.; Kohlmann, S.; Welkerling, P. *Chem. Phys. Lett.* **1985**, *118*, 431.
(57) Kaim, W.; Doslik, N.; Frantz, S.; Sixt, T.; Wanner, M.; Baumann, F.; Denninger, G.; Kummerer, H. J.; Duboc-Toiac, C.; Fiedler, J.; Zalis, S. *J. Mol. Struct.* **2003**, *656*, 183.

(58) Pap, J. S.; George, S. D.; Berry, J. F. *Angew. Chem., Int. Ed.* **2008**, *47*, 10102.

(59) Kuan, S. L.; Tay, E. P. L.; Leong, W. K.; Goh, L. Y.; Lin, C. Y.; Gill, P. M. W.; Webster, R. D. *Organometallics* **2006**, *25*, 6134.

(60) Flanagan, H. L.; Singel, D. J. *J. Chem. Phys.* **1987**, *87*, 5606.

(61) Fittipaldi, M.; Wijma, H. J.; Verbeet, M. P.; Canters, G. W.; Groenen, E. J. J.; Huber, M. *Biochem.* **2005**, *44*, 15193.

(62) Schweiger, A.; Jeschke, G. *Principles of Pulse Electron Paramagnetic Resonance*; Oxford University Press: Oxford, U.K., 2001.

(63) Kasumaj, B.; Stoll, S. *J. Magn. Reson.* **2008**, *190*, 233.

(64) Potapov, A.; Goldfarb, D. *Inorg. Chem.* **2008**, *47*, 10491.

(65) Mims, W. B. *Proc. R. Soc. A* **1965**, *283*, 452.

(66) Carrington, P. J.; Doggett, G. *Mol. Phys.* **1975**, *30*, 49.

(67) *Magnetic Atoms and Molecules*; Weltner, W., Jr., Ed.; Dover Publications Inc.: New York, 1983.

(68) Yang, X.; Baik, M. H. *J. Am. Chem. Soc.* **2006**, *128*, 7476.

(69) Lundberg, M.; Blomberg, M. R. A.; Siegbahn, P. E. M. *Inorg. Chem.* **2004**, *43*, 264.

(70) Batista, E. R.; Martin, R. L. *J. Am. Chem. Soc.* **2007**, *129*, 7224.

(71) Nyhlen, J.; Duan, L.; Aakermark, B.; Sun, L.; Privalov, T. *Angew. Chem., Int. Ed.* **2010**, *49*, 1773.

(72) Yamaguchi, K.; Shoji, M.; Saito, T.; Isobe, H.; Nishihara, S.; Koizumi, K.; Yamada, S.; Kawakami, T.; Kitagawa, Y.; Yamanaka, S.; Okumura, M. *Int. J. Quantum Chem.* **2010**, *110*, 3101.

(73) Sameera, W. M. C.; McKenzie, C. J.; McGrady, J. E. *Dalton Trans.* **2011**, *40*, 3859.

(74) de Oliveira, F. T.; Chanda, A.; Banerjee, D.; Shan, X.; Mondal, S.; Que, L.; Bominaar, E. L.; Münck, E.; Collins, T. J. *Science* **2007**, *315*, 835.

(75) Poppe, J.; Moscherosch, M.; Kaim, W. *Inorg. Chem.* **1993**, *32*, 2640.

(76) Kaim, W. *Coord. Chem. Rev.* **1987**, *76*, 187.

(77) Kaim, W.; Ernst, S.; Kasack, V. *J. Am. Chem. Soc.* **1990**, *112*, 173.

(78) Dengel, A. C.; Griffith, W. P. *Inorg. Chem.* **1991**, *30*, 869.

(79) Yamada, H.; Siems, W. F.; Koike, T.; Hurst, J. K. *J. Am. Chem. Soc.* **2004**, *126*, 9786.

(80) Ozkanlar, A.; Cape, J. L.; Hurst, J. K.; Clark, A. E. *Inorg. Chem.* **2011**, *50*, 8177.

(81) Stich, T. A.; Whittaker, J. W.; Britt, R. D. *J. Phys. Chem. B* **2010**, *114*, 14178.

(82) Besson, C.; Mirebeau, J.-H.; Renaudineau, S.; Roland, S.; Blanchard, S.; Vezin, H.; Courillon, C.; Proust, A. *Inorg. Chem.* **2011**, *50*, 2501.

(83) DeRose, V. J.; Telser, J.; Anderson, M. E.; Lindahl, P. A.; Hoffman, B. M. *J. Am. Chem. Soc.* **1998**, *120*, 8767.

(84) Schafer, K. O.; Bittl, R.; Zweygart, W.; Lendzian, F.; Haselhorst, G.; Weyhermuller, T.; Wieghardt, K.; Lubitz, W. *J. Am. Chem. Soc.* **1998**, *120*, 13104.

4586

dx.doi.org/10.1021/ic4001158 | *Inorg. Chem.* 2013, 52, 4578–4586